Contents lists available at [ScienceDirect](https://www.sciencedirect.com)

Journal of the Mechanics and Physics of Solids

journal homepage: www.elsevier.com/locate/jmps

Defect Sensitivity of Truss Strength

Ryan M. Latture, Matthew R. Begley, Frank W. Zok*

Materials Department, University of California, Santa Barbara, CA 93106, United States



ARTICLE INFO

Article history:

Received 11 June 2018
Revised 9 October 2018
Accepted 23 October 2018
Available online 2 November 2018

Keywords:

Cellular solids
(A) fracture
(A) stress concentrations
(C) finite elements

ABSTRACT

Periodic trusses with missing or defective struts may exhibit reduced strength relative to those of otherwise pristine trusses. The principal goal of the present study is to determine the extent to which individual strut defects and free surfaces, both separately and together, elevate strains in neighboring struts and, in turn, the effects of strain elevations on truss strength, especially in trusses made from elastic-brittle materials. The goals are pursued through finite element analyses of three stretch-dominated truss structures with low relative density under uniaxial compressive loading. In all cases considered, strain elevations due to bulk defects (distant from free surfaces) are comparable to or lower than those associated with the surfaces themselves. Although defects located at truss corners and truss edges cause the highest elevations in strut strains, their effects on truss strength are small (5–25%). Guidelines are presented for the minimal tensile fracture strain of the constituent material required to achieve the full strength potential of the truss, dictated by large-scale strut buckling.

© 2018 Elsevier Ltd. All rights reserved.

1. Introduction

Well-designed periodic trusses exhibit specific stiffness and specific strength that are superior to those of stochastic foams (Bauer et al., 2014; Gurtner and Durand, 2014; Latture et al., 2018a; Messner, 2016; Wadley et al., 2003). They can also be designed for high energy absorption capacity (Asadpoure et al., 2017; Evans et al., 2010; Hammetter et al., 2013; Ostos et al., 2012; Tancogne-Dejean et al., 2016; Zheng et al., 2012). Although complex by standards of conventional manufacturing operations, periodic trusses with almost any topology can now be made by one of numerous additive manufacturing (AM) routes. Indeed, AM has enabled fabrication of previously-unimaginable structures over length scales ranging from micrometers to meters.

The present study addresses one specific aspect of truss performance: that of defect sensitivity of compressive strength. It is motivated by numerous studies showing that truss properties often fall short of theoretical predictions, a consequence of defects and imperfections introduced during manufacturing. In one study, effects of strut waviness in woven metal trusses were found to produce a knock-down in compressive stiffness and compressive strength of about 20% relative to those obtained in corresponding structures with straight struts (Queheillalt et al., 2007). Such effects are well-predicted by analytical and finite element models that account for deviations in strut orientations relative to their ideal values and the resulting axial and bending stresses produced within these struts. In another, variations in strut geometry in hollow-microtube truss structures were measured and the results used to build a stochastic model of geometric imperfections (Salari-Sharif et al., 2018). In turn, through Monte Carlo simulations and finite element analyses, the critical buckling loads were computed for

* Corresponding author.

E-mail address: zok@ucsb.edu (F.W. Zok).

many instantiations of strut geometry. The results were used to rationalize large deviations in strength from the theoretical values for perfectly uniform trusses as well as large statistical strength variations from sample to sample. Yet other studies have found imperfections in the form of progressive changes in strut diameter and local strut properties in polymeric trusses made by a self-propagating photocuring method (Rinaldi et al., 2012; 2013). Analogous effects of geometric imperfections on the mechanical response of solid-strut Ti-alloy trusses fabricated by selective electron beam melting (Campoli et al., 2013) and selective laser melting (Liu et al., 2017) have also been reported. In another computational study, the stiffness and yield strength of an octet-truss panel were found to decrease approximately linearly with the fraction of struts removed from the truss (Wallach and Gibson, 2001). Similar results have been reported for the effects of missing wall members on the modulus, elastic buckling strength and plastic collapse strength of Voronoi honeycombs (Silva and Gibson, 1997) and hexagonal honeycombs (Guo and Gibson, 1999).

Defect sensitivity of truss properties may also be affected by the predominant deformation mode: that is, whether the truss is stretch-dominated or bend-dominated. For example, the elastic moduli of 2-dimensional triangular trusses are minimally affected by random removal of struts (Liu and Liang, 2012; Symons and Fleck, 2008). This is because the starting truss is stretch-dominated and, in the presence of a small number of defects, remains essentially stretch-dominated for all loading states. In contrast, the behavior of 2-dimensional hexagonal trusses depends on the nature of the macroscopic stress state. When loaded in shear, the truss is bend-dominated and therefore its shear modulus is extremely low; removing struts only reduces the shear modulus slightly (Symons and Fleck, 2008). But, when loaded hydrostatically, it deforms entirely by strut stretching. Here, removal of even a small number of struts triggers a transition from stretch- to bend-dominated deformation and a precipitous drop in the bulk modulus (Chen et al., 1999). For example, when 10% of struts are randomly removed from such a truss, the computed bulk modulus decreases by nearly three orders of magnitude (Symons and Fleck, 2008).

Viewed from a different perspective, the extent to which defects affect truss properties may be influenced by the nature of the failure mechanism. For example, if the load-bearing capacity is dictated by *elastic strut buckling*, the presence of a small number of missing struts should not significantly affect truss strength. Although missing struts may cause strain elevations in neighboring struts and lead to premature buckling of the affected struts, eventually all remaining compressive struts also buckle, each supporting *nominally* the same load. In this case, the truss strength is reduced by an amount proportional to the fraction of missing struts (Wallach and Gibson, 2001). In contrast, if failure occurs by *brittle fracture* of struts that experience tensile stresses, the strain elevations around a single missing strut may initiate fracture of neighboring struts, possibly leading to a cascade of further strut fractures and ultimately complete truss failure. Here, the load-bearing capacity of the truss would be determined by extreme values of tensile stresses within the struts and would follow weakest link scaling laws. Failure via *plastic strut yielding* is likely to exhibit an intermediate sensitivity to strut defects. That is, local strain elevations may trigger strut yielding in regions adjacent to strut defects which, in turn, may lead to *plastic* buckling before the remaining struts have yielded. Because of the strain softening inherent to plastic buckling, the process is likely not as benign as elastic buckling (where buckled struts sustain essentially a constant load); but it is likely to spread in a more progressive manner relative to that associated with strut fracture (where failed struts have no load-bearing capacity).

Free surfaces of trusses are, themselves, defects. Because of reduced nodal connectivity at surfaces, strut strains may be elevated relative to those in the bulk (Fleck and Qiu, 2007). Finite element simulations for the {FCC} (octet) truss have shown that struts oriented perpendicular to the loading direction and situated along the edges experience strains that are as much as 50% greater than those of equivalent struts in the bulk (Lattice et al., 2018a; Messner, 2016). These strain elevations have been confirmed by experimental measurements of strut strains using digital image correlation (Lattice et al., 2018b). These measurements also confirm that the strains in the affected tensile struts are almost entirely due to axial deformation; the contributions from bending are negligible, as predicted by the simulations. They further show that the strains in compressive struts situated at the truss corners experience significant bending, with bending strains comprising up to 50% of the peak principal strut strains.

The goal of the present study is to determine the effects of individual strut defects and free surfaces, both separately and together, on strains in neighboring struts and the effects of strain elevations on the strength of three elastic-brittle, stretch-dominated truss structures. The article is organized in the following way. The truss topologies and defect types are described in Section 2. Finite element (FE) models are described in Section 3. Results for strut strain distributions in the elastic (pre-buckling) domain are summarized in Section 4. The nonlinear responses of the trusses, wherein struts buckle and/or fail in tension, are presented in Section 5. The implications for truss design and topology selection are noted in Section 7.

2. Truss topologies and defect types

The three truss structures of present interest are: (i) the octet truss, denoted $\{nFCC\}^3$, (ii) the binary truss $60\% \{nBCC\}^3 | 40\% \{nSC\}^3$; and (iii) the binary truss $80\% \{nFCC\}^3 | 20\% \{nSC\}^3$. Here {BCC}, {SC} and {FCC} refer to the elementary trusses based on body-centered cubic, simple cubic and face-centered cubic lattices, respectively; the percentages refer to volume fractions of material allocated to the constituent elementary trusses; the exponent 3 denotes that unit cells are tiled in 3 dimensions; and n is the lineal number of unit cells in each of the three tiling directions (Zok et al., 2016). Examples of the three trusses, each with $n = 2$, are shown in Fig. 1.

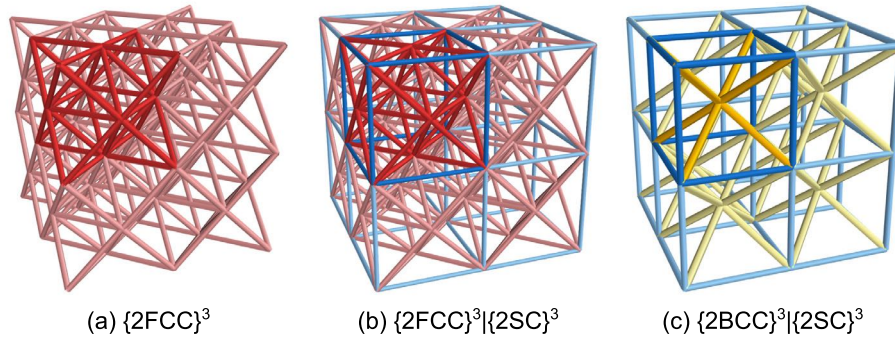


Fig. 1. Cubic truss structures at a relative density $\rho = 0.05$. Unit cells are indicated by darker colors.

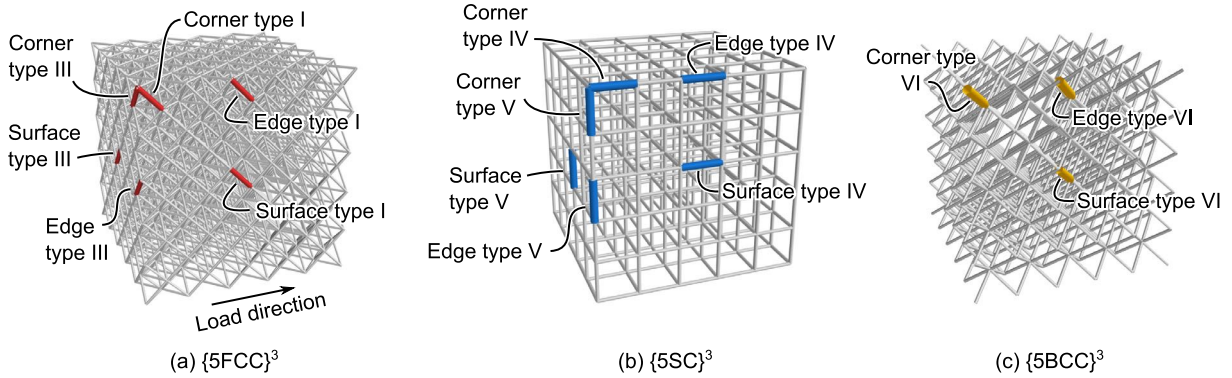











Fig. 2. Locations of surface, edge and corner defects in (a) $\{5FCC\}^3$, (b) $\{5SC\}^3$ and (c) $\{5BCC\}^3$ trusses.

The two binary trusses are elastically isotropic and exhibit the maximal possible stiffness for strut-based trusses. Their elastic properties are $E/E_0\rho = 1/6$, $G/E_0\rho = 1/15$ and $\nu = 1/4$, where ρ is relative density, E is Young’s modulus, G is shear modulus, ν is Poisson’s ratio, and E_0 is the Young’s modulus of the parent material (Gurtner and Durand, 2014; Latture et al., 2018a). In contrast, the $\{nFCC\}^3$ truss is elastically anisotropic, with Young’s moduli varying from a low of $E/E_0\rho = 1/9$ in $[100]$ -type directions to a high of $E/E_0\rho = 1/5$ in $[111]$ -type directions (Deshpande et al., 2001).

Strut types are denoted according to the system laid out in (Latture et al., 2018a). In $\{FCC\}$ trusses, type I struts are aligned with $[110]$ and $[\bar{1}\bar{1}0]$ directions, type II are aligned with $[101]$ and $[\bar{1}0\bar{1}]$ directions, and type III are aligned with $[011]$ and $[0\bar{1}\bar{1}]$ directions. Under compressive loading along the $[100]$ direction, both type I and type II struts are oriented at 45 degrees to the compression direction and experience equivalent compressive strains. (The distinction between type I and type II struts is only necessary when considering shear loading, wherein the two strut types are loaded in opposite directions: one in compression and the other in tension. For compressive loading, both are treated as type I struts.) Type III struts are perpendicular to the compression direction and experience axial tension. In $\{SC\}$ trusses, type IV struts are aligned with the $[100]$ (loading) direction while type V struts are aligned with the $[010]$ and $[001]$ directions: the latter being loaded in tension when the truss is loaded in compression along the $[100]$ direction. In $\{BCC\}$ trusses, type VI struts are aligned with $[111]$ and $[\bar{1}\bar{1}\bar{1}]$ directions while type VII are aligned with $[1\bar{1}\bar{1}]$ and $[11\bar{1}]$ directions. (Here again the distinction between the two strut types is only necessary for shear loading. In compression the two are identical and are treated here as type VI struts.) Table 1 shows struts of each type and their axial strains in an infinite truss ($n = \infty$) (Latture et al., 2018a).

Defect types are similarly denoted by the type of missing strut (I, III, IV, V and VI). Defects are further distinguished by their locations: *bulk* defects being in the truss interior (far from the free surfaces), *surface* defects on one of the external faces parallel to the loading direction, *edge* defects at the intersections of two external faces, and *corner* defects at one of the 8 truss corners. In the subsequent analyses, surface defects are placed at the center of one of the external faces and edge defects are placed along the mid-point of an edge. Locations of surface, corner and edge defects are shown in Fig. 2.

Table 1
Strut types and axial strut strains for uniaxial compressive loading.

	{SC}		{BCC}		{FCC}	
	Strut type	$\frac{\epsilon_a}{\epsilon_1}$	Strut type	$\frac{\epsilon_a}{\epsilon_1}$	Strut type	$\frac{\epsilon_a}{\epsilon_1}$
80% {FCC} 20% {SC}	{FCC}	—	—	—	I	 $\frac{1}{3}$
					III	 $-\frac{1}{3}$
	IV	 1	—	—	I	 $\frac{3}{8}$
	V	 $-\frac{1}{4}$			III	 $-\frac{1}{4}$
60% {BCC} 40% {SC}	IV	 1	VI	 $\frac{1}{6}$	—	—
	V	 $-\frac{1}{4}$				

3. Finite element methods

Trusses were discretized using Timoshenko beam elements with circular cross-section. All struts of each elementary truss were assigned equal cross-sectional area, determined by the volume fractions of the constituent trusses. The strut material was assumed to be linear elastic up to fracture. Simulations were performed for trusses with relative densities $\rho = 0.01$ or 0.05 , although the normalizations introduced below allow the results to be generalized for other values of relative density. Defects were introduced by removing individual struts of the designated type. Compressive loads were applied along the [100] direction, hereafter denoted as the 1-axis. Models were processed using the commercial package Abaqus (Version 6.13-EF4, Dassault Systèmes, Providence, Rhode Island).

Both linear and non-linear simulations were performed. For the linear simulations, nodal displacements were prescribed on opposing faces of the model: $u = \epsilon_1 L$ at $x = L$ and $u = 0$ at $x = 0$, where u is nodal displacement along the 1-axis, x is the position on the 1-axis, ϵ_1 is the strain in the 1-direction and L is the length of the truss along the principal directions. This yields uniaxial compressive loading along the [100] direction.

For the nonlinear simulations (incorporating effects of elastic strut buckling), nodal velocities (instead of displacements) were prescribed on one face: $\dot{u} = \dot{\epsilon} L$ at $x = L$ where the dots represent derivatives with respect to time. The opposing face was fixed ($u = 0$ at $x = 0$). Rigid body motion was prevented by pinning the node at the origin, i.e. $u = v = w = 0$ at $(0, 0, 0)$ where v and w are nodal displacements in the 2- and 3-directions, respectively, and by assigning $w = 0$ to the node at $(0, L, 0)$. Velocities were selected to yield quasi-static strain rates ($|\dot{\epsilon}| = 10^{-3} s^{-1}$). To reduce computation time, the mass density in the nonlinear simulations was artificially increased by a factor of 10. To minimize oscillations following tensile failure, damping was introduced in the form of linear bulk viscosity. The viscosity generates a pressure, $p = \xi \rho_0 c_d l_e \dot{\epsilon}_{vol}$, where ξ is a damping coefficient (taken to be $\xi = 0.48$), ρ_0 is mass density, c_d is the dilatational wave speed, l_e is the length of the element and $\dot{\epsilon}_{vol}$ is the volumetric strain rate. To confirm that the loading was quasi-static (prior to strut failure), the ratio of kinetic energy to potential energy was computed at each time step and found to be less than 10^{-2} .

Two truss sizes were studied. The first, with $n = 11$, was used to assess the effects of bulk defects in essentially infinite trusses. Here strut defects were placed at the truss center. Using linear simulations, the principal strains in all struts in both the pristine and the defect-containing trusses were calculated from the strain components derived from axial, bending and torsional deformation modes on the strut surfaces. We find, however, that maximum principal strains in the linear elastic

domain are dominated by axial strains; bending and torsional modes contribute minimally. The size of the affected region around the bulk defects was characterized by the distance from the centroid of the defect to the centroid of the farthest strut in which the principal strains differ by at least 5% relative to that in the same strut within a pristine truss.

A second set of linear simulations was performed for $n = 5$. In this case, defects were placed on either bulk, surface, edge or corner sites. Here again the principal strains were computed for all struts in both pristine and defect-containing trusses. The objective of these simulations was to ascertain, both separately and together, the effects of free surfaces and strut defects on local strut strains. Because of reduced nodal connectivity of struts at free surfaces, such struts also experience strain elevations. In this context, surfaces themselves serve as defects, competing with missing struts to determine which ultimately dictates strength.

Results for peak values of maximum and minimum principal strains, ϵ_{max} and ϵ_{min} , respectively, are couched in two normalized forms. For tensile struts they are $k_{max} \equiv \epsilon_{max}/\epsilon_{max}^0$ and $\epsilon_{max}/\epsilon_1 = k_{max}\epsilon_{max}^0/\epsilon_1$ where ϵ_{max}^0 is the maximum strain that would be obtained in an equivalent strut in the absence of a defect, ϵ_1 is the macroscopic axial strain, and k_{max} is the strain concentration factor; for the compressive struts they are $k_{min} \equiv \epsilon_{min}/\epsilon_{min}^0$ and $\epsilon_{min}/\epsilon_1 = k_{min}\epsilon_{min}^0/\epsilon_1$ where ϵ_{min}^0 is the largest minimum principal strain that would be obtained in an equivalent strut in the absence of a defect and k_{min} is the corresponding strain concentration factor. Although the former of each pair (the strain concentration factors) represent the relative effects of defects on the neighboring fields, the latter of each pair, when compared to values for other struts in the same truss, provide a more informative indicator of which defects are likely to dominate failure.

To determine the separate effects of free surfaces and strut defects, strut strains are also couched in terms of minimum and maximum principal strains due to free surfaces, ϵ_{min}^{edge} and ϵ_{max}^{edge} , and those due to a single strut defect, ϵ_{min}^{defect} and ϵ_{max}^{defect} . When $\epsilon_{max}^{defect}/\epsilon_{max}^{edge} < 1$, bulk strut defects are not expected to be strength-limiting.

All nonlinear simulations were performed for $n = 5$ (larger truss sizes being somewhat prohibitive in terms of computation time). Although the size of the truss is smaller than that of the linear simulations, strain amplification due to free surface effects are nearly equivalent to those of the larger truss (Latture et al., 2018a). The goal of these simulations was to determine the effects of defects on both buckling of struts in compression and fracture of struts in tension. Tensile fracture was assumed to occur when the maximum principal strain in the tensile struts exceeds a critical value at any point in an element. The broken element was then removed from the model.

To accurately determine the sequence of strut fractures, the nonlinear simulations were performed in two steps. In the first, the state of the system was recorded at 100 equally-spaced time increments, up to a macroscopic strain of 1%. From this data, the increment of time (usually within a single time step) over which most failures occurred was identified. The simulations were then repeated, in this case with the state of the system being saved in 1000 equally-spaced time increments within the interval in which the failure events occurred.

In order to probe transitions from buckling-dominated to fracture-dominated domains, the tensile failure strains selected for this study were based on the expected strains required for strut buckling, using the {FCC} truss as a baseline, in the following way. In the {FCC} truss, type I struts buckle at an axial strut strain $\epsilon_a = \rho/6$, essentially independent of truss size (Latture et al., 2018a). Within the bulk of a large truss, the axial tensile strains in type III struts are of equal magnitude ($\epsilon_a = \rho/6$). At free surfaces, however, the reduced nodal connectivity leads to a 50% elevation in strut strain, yielding $\epsilon_a = \rho/4$ (Latture et al., 2018b). Neglecting bending strains, the expectation therefore is that, when the tensile failure strain is $\epsilon_f = \rho/4$, buckling of type I struts and tensile failure of near-surface type III struts should occur simultaneously. Accordingly, most simulations were performed using one of four tensile failure strains: two below and two above the expected critical value, notably $\epsilon_f/\rho = 0.048, 0.24, 0.48$ or 0.96 . The same values of fracture strains were employed for all truss types. To capture the transition from fracture- to buckling-dominated failure in each truss, additional FE simulations were performed with ϵ_f/ρ ranging from 0.097 to 1.34. Baseline simulations were also performed without a prescribed failure strain, i.e. for a purely linear-elastic material.

The results are expressed in terms of stress normalized by $E_0\rho^2$ and strain normalized by ρ (Latture et al., 2018a). These normalizations yield the expected scalings in properties: notably, stiffness proportional to $E_0\rho$ and buckling strength proportional to $E_0\rho^2$. Provided ρ is sufficiently small and failure is buckling-dominated (that is, neither yielding nor fracture intervene), the results in this form are, to a very good approximation, independent of ρ and E_0 .

4. Elastic strain concentrations

4.1. Role of free surfaces

The maximum tensile strains in the {FCC} truss (absent defects) are obtained in type III struts located along the truss edges (arrows in Fig. 3a). Here the peak strains and strain concentrations are $\epsilon_{max}/\epsilon_1 = -0.51$ and $k_{max} = 1.53$ (Table 3). But the effects are highly localized; neighboring struts experience only slight strain elevations while those more than 2 strut lengths from the defect location are almost unaffected.

The maximum tensile strains in the {FCC}{SC} truss also occur in type III struts located near the truss edges, but offset by a distance of one strut length from the edge itself (arrows in Fig. 3b). Here the peak strains are considerably smaller: $\epsilon_{max}/\epsilon_1 = -0.36$ (Table 3). Strain elevations are also obtained in the type V struts within the {SC} sub-truss located along the free surfaces, although their magnitudes are even smaller ($\epsilon_{max}/\epsilon_1 = -0.28$). In the {BCC}{SC} truss, the peak tensile strains

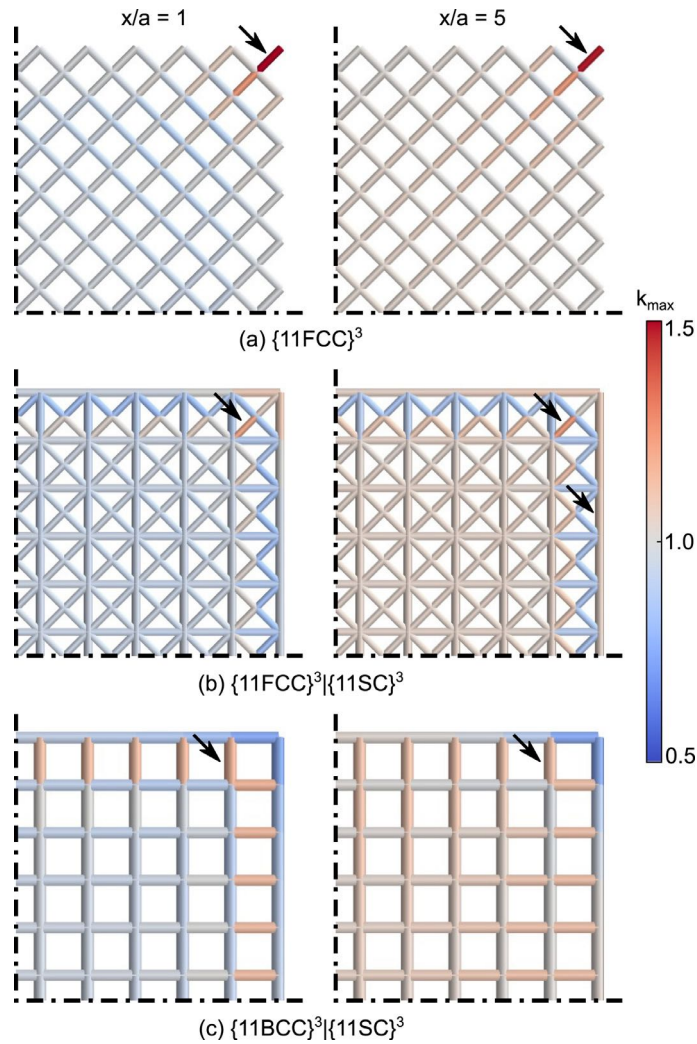


Fig. 3. (a) The greatest strain concentrations in tensile struts within the $\{FCC\}$ truss are largely confined to the edge struts (shown here in cross-sections transverse to the loading directions, at two distances from one of the loaded faces: $x/a = 1$ and 5). (b, c) The greatest strain concentrations in the two binary trusses are similarly obtained at the truss edges, but their magnitudes are somewhat smaller. Arrows indicate struts with the maximum strain concentration factor within each plane. Due to the cubic symmetry of the trusses, only one quadrant of each cross-section is shown. Thick dashed lines indicate lines of symmetry. [Videos showing sections at distances that, in totality, comprise data for all tensile members in the truss can be found in Supplementary Information (Vid. S1-S3).]

are obtained in type V struts located at the free surface and oriented perpendicular to those surfaces ($\epsilon_{max}/\epsilon_1 = -0.29$, Fig. 3c, Table 3).

4.2. Bulk defects in infinite trusses

As we show presently, elevations in the minimum principal strains around strut defects do not affect the buckling response and thus the following discussion focuses on tensile struts alone. (Notwithstanding, the minimum principal strains may be relevant to scenarios in which failure involves strut yielding and are therefore included for completion, in Tables 2 and 3).

Bulk defects are most benign in the $\{FCC\}$ truss (Tables 2 and 3). The maximum tensile strains in type III struts increase by 25% and 12% around type I and type III defects, respectively. The strain elevations persist over distances of 2 strut lengths (or 1.4 unit cell lengths). Most importantly, the strain elevations are smaller than those in struts located at the free surfaces. The inference is that, when truss failure is fracture dominated, bulk defects should play almost no role in truss strength.

In the binary trusses, only type IV defects (within the $\{SC\}$ truss) result in peak tensile strains that exceed those due to free surfaces. In the $\{FCC\}\{SC\}$ truss, peak tensile strains (in type III struts) increase by 50% around a type IV defect,

Table 2

Struts with at least a 5% change in principal strain due to the presence of a defect (shown in black). Colors of intact struts represent minimum or maximum principal strut strains.

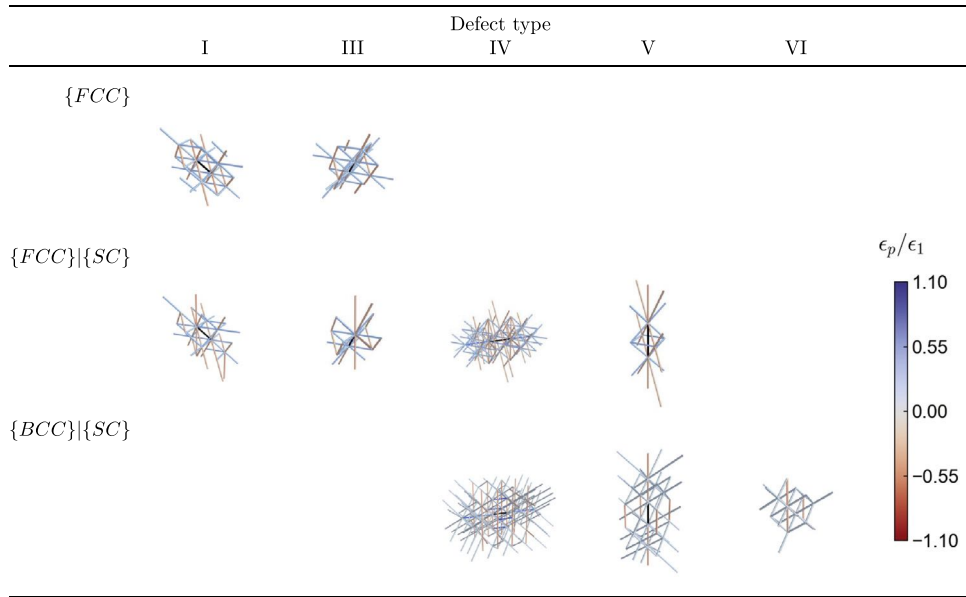


Table 3

Effects of bulk defects on principal strut strains.

Truss	Defect type	Strut type									
		I, II		III		IV		V		VI, VII	
		$\frac{\epsilon_{min}}{\epsilon_1}$	$\frac{\epsilon_{min}^{defect}}{\epsilon_{min}^{edge}}$	$\frac{\epsilon_{max}}{\epsilon_1}$	$\frac{\epsilon_{max}^{defect}}{\epsilon_{max}^{edge}}$	$\frac{\epsilon_{min}}{\epsilon_1}$	$\frac{\epsilon_{min}^{defect}}{\epsilon_{min}^{edge}}$	$\frac{\epsilon_{max}}{\epsilon_1}$	$\frac{\epsilon_{max}^{defect}}{\epsilon_{max}^{edge}}$	$\frac{\epsilon_{min}}{\epsilon_1}$	$\frac{\epsilon_{min}^{defect}}{\epsilon_{min}^{edge}}$
{FCC}	—	0.509		-0.505							
	I, II	0.468	0.919	-0.416	0.825						
	III	0.466	0.917	-0.372	0.737						
{FCC}{SC}	—	0.559		-0.356		1.061		-0.274			
	I, II	0.501	0.896	-0.332	0.933	1.067	1.006	-0.303	1.108		
	III	0.475	0.849	-0.276	0.775	1.022	0.963	-0.296	1.083		
	IV	0.656	1.173	-0.375	1.053	1.027	0.968	-0.288	1.053		
	V	0.475	0.850	-0.316	0.887	1.022	0.963	-0.264	0.963		
{BCC}{SC}	—					1.052		-0.293		0.358	
	IV					1.077	1.024	-0.335	1.145	0.446	1.246
	V					1.035	0.984	-0.279	0.951	0.278	0.776
	VI, VII					1.039	0.988	-0.291	0.995	0.258	0.722

Shaded numbers are those most relevant to discussion in the text.

exceeding the maximum tensile strain at the edges by 5%. In the {BCC}{SC} truss, the peak tensile strains due to a type IV defect exceed those due to the free surfaces by about 15%.

4.3. Defects in finite trusses

The effects of defects in finite trusses depend on defect location (Fig. 4). In the {FCC}³ truss, the effects of a center defect are identical to those at the center of the larger ({11FCC}³) truss (Tables 2 and 4); both yielding peak strains lower than those at the free surfaces. Defects at corners, edges and surfaces are similarly benign.

In the {BCC}{SC} truss, type IV defects have the greatest effect, with the strains in surrounding struts being greater than that due to the surfaces for all defect locations (Fig. 5). Among the possible locations, the edge site is most deleterious; the local strut strain there is about 19% greater than that at the free surfaces in the absence of defects. In the {FCC}{SC} truss,

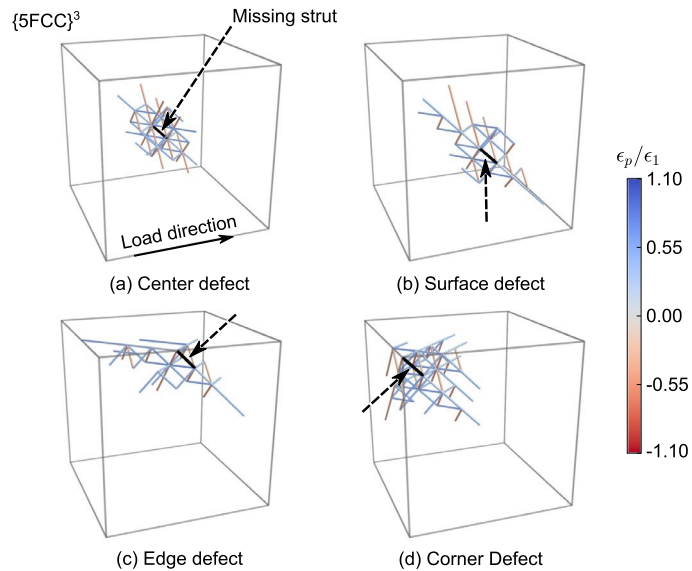


Fig. 4. Strain elevations around type I strut defects in the $\{FCC\}^3$ truss depend on defect location, the maximum occurring when the defect is at a truss corner. The effects persist over distances of about two strut lengths. Only struts that experience a strain change $\geq 5\%$ are shown. Arrows indicate missing struts.

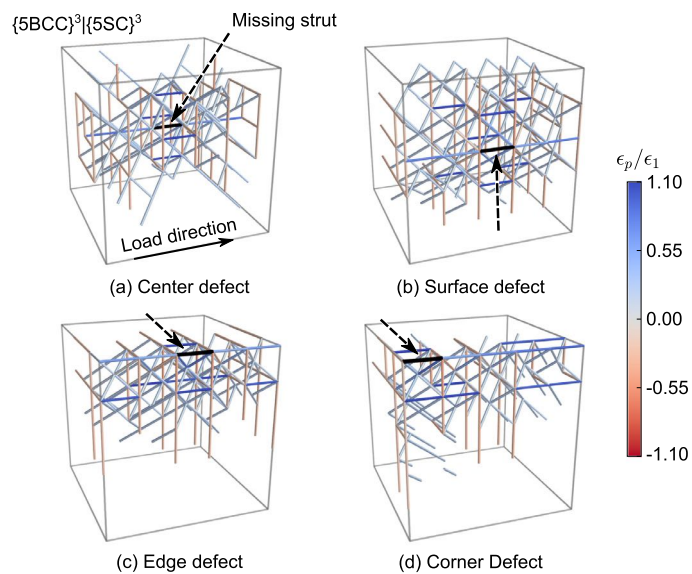


Fig. 5. Strain elevations around type IV strut defects in the $\{5BCC\}^3\{5SC\}^3$ truss depend on defect location. Although the strain concentrations are modest, they persist over lengths approaching (in this case) the entire truss. Only struts that experience a strain change $\geq 5\%$ are shown. Arrows indicate missing struts.

type I and type IV defects also yield local strains exceeding those of the free surfaces. The most extreme case is that of a type IV edge defect; the local strains there are 59% greater than those due to the free surfaces alone.

5. Failure response of finite trusses

Coupled effects of defect type, defect location and tensile failure strain on the compressive stress-strain response of the three trusses are shown in Fig. 6. Two combinations of defect type and defect location were considered for each truss type. The selected combinations produce the greatest tensile strain elevations (Table 4). The variation in truss strength with failure strain (absent strut defects) is plotted on Fig. 7.

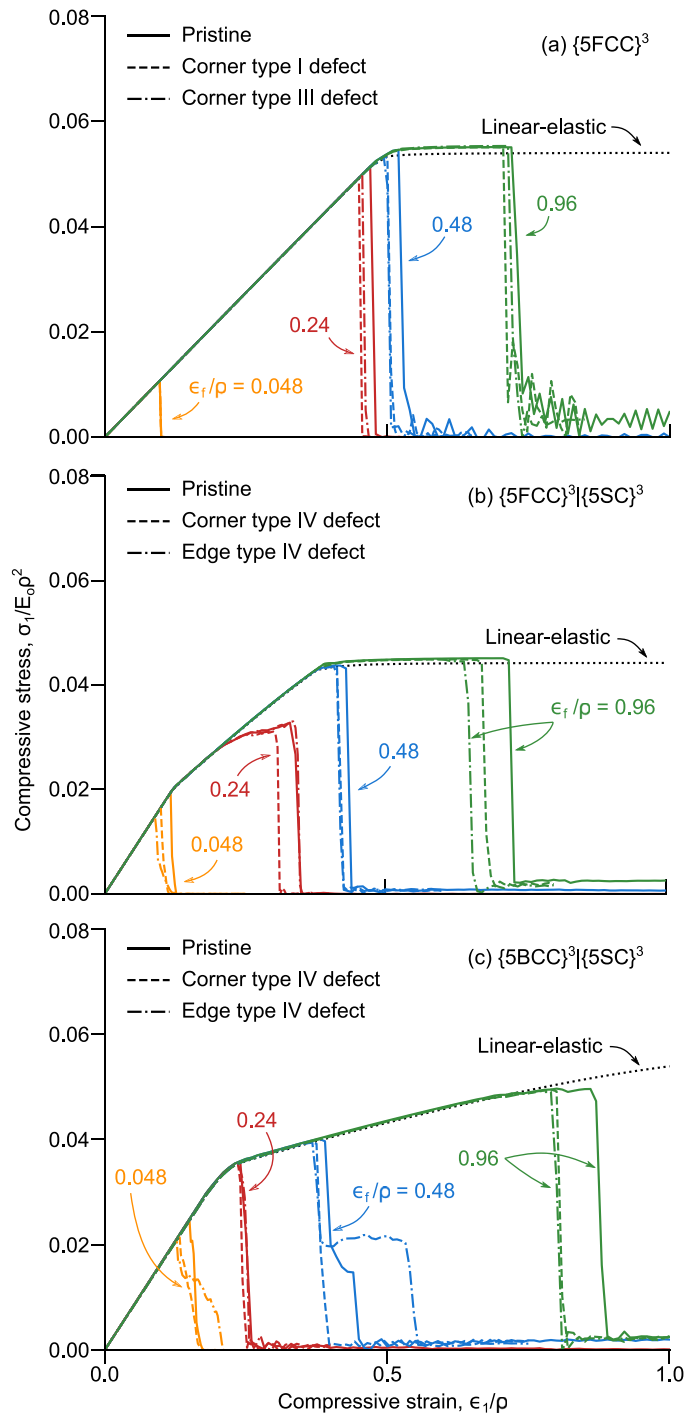


Fig. 6. Stress-strain responses of the three trusses exhibit varying degrees of non-linearity, dependent on truss topology and material failure strain; the presence of strut defects and their locations within the truss play secondary roles. (a) The $\{5FCC\}^3$ truss undergoes a single buckling event at essentially a single stress, thereby producing effectively elastic-“perfectly plastic” response. (b, c) The two binary trusses undergo two buckling events, each associated with one of the two compressive strut populations. (The second buckling event in the $\{5BCC\}^3\{5SC\}^3$ truss occurs slightly beyond the maximum strain shown, at about $\epsilon_1/\rho \approx 1.5$.)

Table 4
Effects of defects on tensile strut strains in finite trusses.

Truss	$\epsilon_{max}^{edge}/\epsilon_1$	Defect type	Defect location	$\epsilon_{max}^{defect}/\epsilon_1$	$\epsilon_{max}^{defect}/\epsilon_{max}^{edge}$
{5FCC} ³	-0.50	I	corner	-0.49	0.99
			edge	-0.47	0.94
			surface	-0.44	0.88
			center	-0.44	0.88
		III	corner	-0.49	0.99
			edge	-0.39	0.78
			surface	-0.38	0.75
			center	-0.39	0.78
{5FCC} ³ {5SC} ³	-0.35	I	corner	-0.43	1.25
			edge	-0.42	1.22
			surface	-0.42	1.19
			center	-0.35	0.99
		III	corner	-0.33	0.94
			edge	-0.28	0.79
			surface	-0.26	0.75
			center	-0.31	0.89
		IV	corner	-0.48	1.39
			edge	-0.55	1.59
			surface	-0.47	1.36
			center	-0.38	1.08
		V	corner	-0.35	1.00
			edge	-0.33	0.94
			surface	-0.27	0.78
			center	-0.32	0.92
{5BCC} ³ {5SC} ³	-0.32	IV	corner	-0.36	1.13
			edge	-0.38	1.19
			surface	-0.35	1.12
			center	-0.35	1.11
		V	corner	-0.28	0.90
			edge	-0.29	0.92
			surface	-0.29	0.90
			center	-0.29	0.92
		VI	corner	-0.28	0.90
			edge	-0.29	0.92
			surface	-0.31	0.98
			center	-0.32	1.01

Shaded numbers are those most relevant to discussion in the text.

5.1. {FCC} truss

The intrinsic response of the {FCC} truss is essentially elastic-“perfectly plastic”. That is, buckling occurs in all compressive struts over a narrow strain range; thereafter, the stress needed for continued buckling remains constant. When the material failure strain is taken as $\epsilon_f/\rho = 0.24$, strut failure initiates essentially at the point of incipient buckling, where the stress-strain curve just begins to display slight non-linearity. Once buckling initiates, bending of the most critically-loaded struts leads to strut fracture. Failure initiates in tensile struts near the corners and then proceeds diagonally along a (111)-type plane (Vid. S4). Corner defects do not alter the failure response, except that the failure initiation site is shifted slightly towards the defect (Vid. S5–S6).

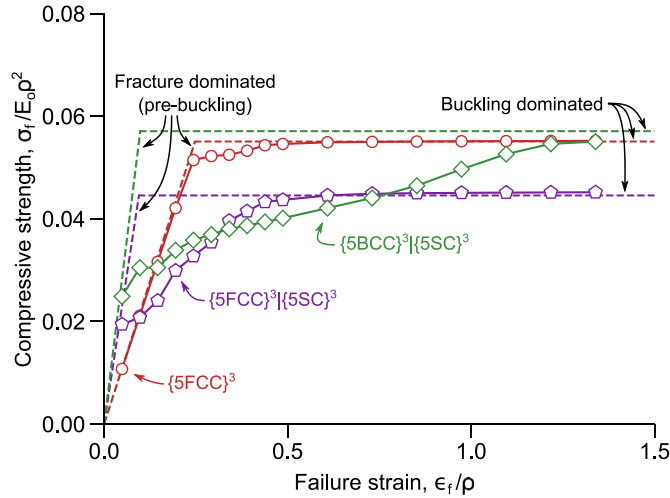


Fig. 7. Compressive strengths of the three trusses transition from being fracture-dominated to buckling-dominated as the material failure strain increases. In the former domain, truss strength is linear with failure strain (indicated by inclined dashed lines, from Eq. 1); in the latter, it is independent of failure strain (indicated by horizontal dashed lines). In the {FCC} truss, the transition occurs over a relatively narrow range of failure strains ($\epsilon_f/\rho = 0.25$ to 0.5). In contrast, the transitions in the two binary trusses are gradual, spanning a range of failure strains of about an order of magnitude (roughly, from $\epsilon_f/\rho = 0.1$ to 1). In the {BCC}|{SC} truss in particular, the failure strain needed to attain the full strength is $\epsilon_f/\rho = 1.5$.

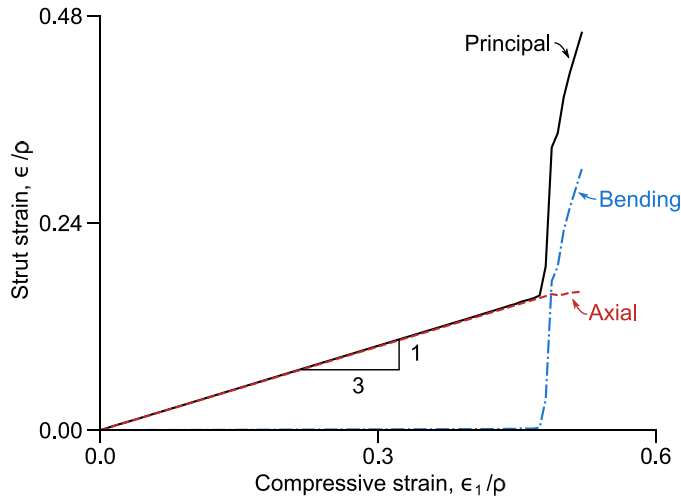


Fig. 8. The principal strain in the first tensile strut to fail in the {FCC} truss is initially due entirely to axial deformation. Once the neighboring compressive struts buckle, the axial strain in the tensile strut remains constant; further increases in the maximum principal strain are due to nodal rotations resulting from buckling and, in turn, to strut bending. The curves terminate once the strut strain reaches its failure strain which, in this case, is $\epsilon_f/\rho = 0.48$.

Doubling the material failure strain (to $\epsilon_f/\rho = 0.48$) increases the truss failure strain by only a small amount. This is because, once large-scale buckling occurs, nodal rotations and corresponding bending strains in the tensile members increase rapidly, bringing those struts to criticality with only small amounts of additional applied strain (Fig. 8). Here again the failure sequence initiates at the corner and proceeds along type III struts within (111)-type planes (Vid. S7). Somewhat larger (though not proportionate) gains in truss failure strain are made when the material failure strain is doubled again (to $\epsilon_f/\rho = 0.96$). In this case, failure occurs well within the plateau associated with large-scale buckling.

In contrast, when the material failure strain is reduced five-fold from the baseline value (that is, from $\epsilon_f/\rho = 0.24$ to $\epsilon_f/\rho = 0.048$), both the failure strain and the failure stress of the truss decrease proportionately. In this domain, failure occurs while the tensile struts experience only axial strains (with minimal bending); since these strains are proportional to the applied strain, it follows that truss strength varies linearly with the material failure strain. Since truss fracture occurs almost immediately after the first strut failure, the ultimate strength is expected to follow in accordance with

$$\sigma_f/E_0\rho^2 = (E/E_0\rho)(\epsilon_1/\epsilon_a k_{max})(\epsilon_f/\rho) \tag{1}$$

where, for the {FCC} truss, $E/E_0\rho = 1/9$, $\epsilon_a/\epsilon_1 = 1/3$ and $k_{max} = 1.5$. This prediction, superimposed on Fig. 7, agrees very well with the computed strengths.

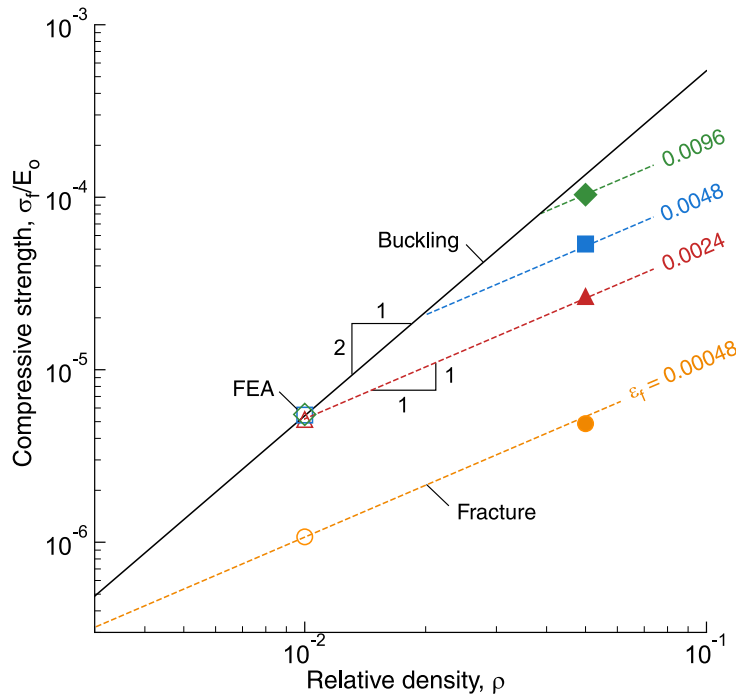


Fig. 9. The compressive failure mode of the {FCC} truss transitions from buckling of the compressive struts to fracture of the tensile struts at a critical point dictated by relative density and material failure strain. Accompanying the transition is a change in the sensitivity of strength to relative density, from quadratic to linear. (Dashed lines are analytical predictions, from Eq. 1; symbols are from FEA.)

The preceding behavioral transition (at a critical material failure strain) is also manifested as the relative density is varied. The latter transition is shown in a plot of strength vs. relative density (Fig. 9). At low values of ρ , the strength is buckling-dominated and proportional to ρ^2 . In contrast, at high values of ρ , the strength is fracture-dominated and proportional to ρ . The transition occurs at a critical value of ρ that depends on material failure strain. From Eq. 1 and the computed buckling strength ($\sigma_f/E_0\rho^2 = 0.056$), the transition is expected at $\epsilon_f/\rho = 0.25$.

Strut defects, even when located in the most deleterious locations, have remarkably small effects on strength of the {FCC} truss (typically $\leq 5\%$). This is because strain concentrations associated with the surfaces are generally greater than those around strut defects.

5.2. Binary trusses

The behaviors of the two binary trusses differ from that of the {FCC} truss in three ways. First, the intrinsic responses of the binaries involve two sets of buckling events: one each for the {SC} and either the {FCC} or {BCC} constituent trusses. The limit stress for the {FCC}{SC} truss is about 20% lower than that of the {FCC} truss. This reflects the volume fraction of material allocated to the {SC} truss, the latter bearing minimal load after buckling. Additionally, the material failure strain needed to reach the limit stress is considerably higher than that in the {FCC} truss. This is because buckling of the first set of struts (within the {SC} truss) induces bending in the tensile struts and therefore accelerates failure. The limit stress for the {BCC}{SC} truss is marginally greater than that of the {FCC} truss. But here again buckling of the {SC} truss (at about 70% of the limit stress) induces bending in the tensile struts. Attaining the full strength potential therefore requires materials with higher failure strains (by a factor of about 5 relative to that needed for the {FCC} truss).

Second, in the domain in which the material failure strain is small, the strength is again proportional to the material failure strain, in accordance with Eq. 1; here $E/E_0\rho = 1/6$ for both binary trusses, and $\epsilon_a/\epsilon_1 = -0.35$ and -0.32 for the {FCC}{SC} and the {BCC}{SC} trusses, respectively. Here the {BCC}{SC} truss emerges as the best choice; the combination of high stiffness and low strains in the constituent tensile struts render it the strongest (more than twice that of the {FCC} truss).

Third, the strengths of the binary trusses exhibit a stronger defect sensitivity when the material failure strain is low. In this domain, a type IV corner defect reduces the compressive strength of the {FCC}{SC} truss by 25%. Fracture initiates at the flaw location. In contrast, in the pristine truss, failure initiates in the type III struts at the truss corners and edges, indicated in Fig. 3. In the {BCC}{SC} truss, type IV edge and corner defects reduce compressive strength by roughly 13 and 16%, respectively. The reductions in strength agree with strain amplifications due to these defects (Table 4). In both defective

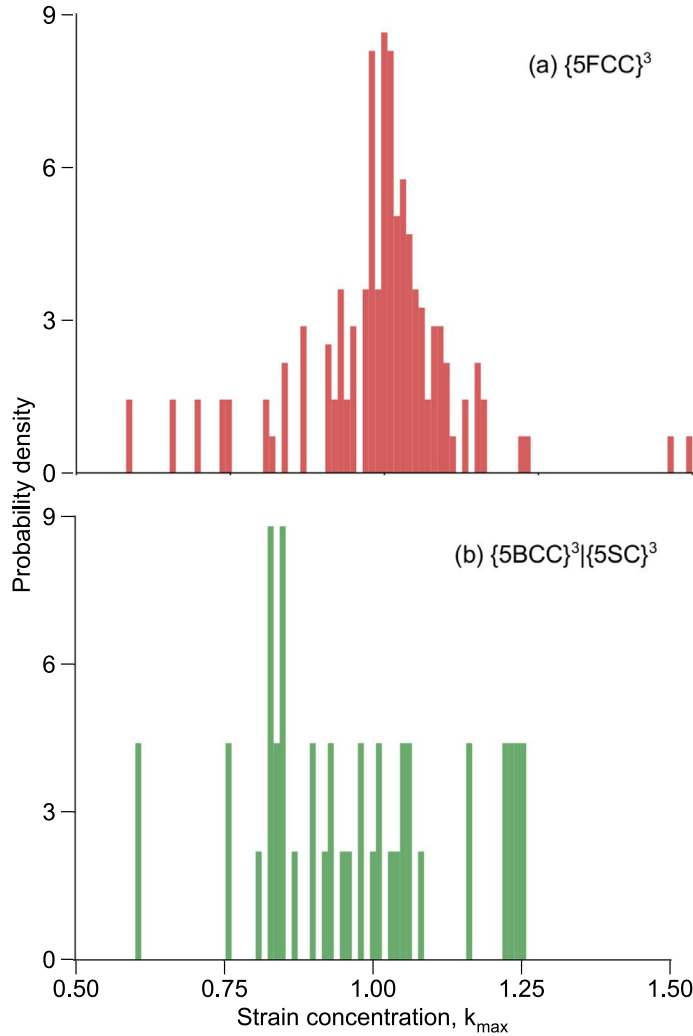


Fig. 10. (a) The maximum principal strain concentrations in the $\{5FCC\}^3$ truss fall in the range of 0.6 to 1.5, although the number density of struts at the high end of this range is exceedingly small. (b) The $\{5BCC\}^3|\{5SC\}^3$ trusses exhibit a somewhat narrower range. Although the peak value is lower (about 1.25), the number density of struts with the highest strains is considerably greater than that in the $\{5FCC\}^3$ truss.

trusses, tensile failure initiates near the defects. [Details of failure sequences are provided in Supplementary Material (Vid. S8-S12).]

5.3. Stochastic failure

Although the present study has focused on cases in which the material failure strain and hence strength are deterministic material properties, some insights into defect sensitivity when failure is stochastic can also be gleaned. Assuming that truss failure occurs when the first tensile strut breaks—an assumption consistent with the FE simulations—the truss strength distribution can be written in terms of the *strut strength* distribution coupled with *strut stress* distribution. Here the survival probability of the truss is simply the product of survival probabilities of all individual struts. If the strength of the struts follows a Weibull distribution with reference strength σ_0 for a reference volume equal to strut volume and with a Weibull modulus (or dispersion index) m , the survival probability P_s can be expressed as (Zok, 2017)

$$\ln P_s = - \sum_{i=1}^N (k_i \sigma_n / \sigma_0)^m \tag{2}$$

where σ_n is the nominal tensile strut stress in an infinite truss, k_i is the stress (or strain) concentration on strut i , and N is the total number of tensile struts. It follows that the ratio of the median strength (corresponding to $P_s = 1/2$) of a finite truss in which surface effects are operative to that of a notional truss of the same size but *without* surface effects is $\langle k_i^m \rangle^{-1/m}$ where $\langle \rangle$ denotes a mean value.

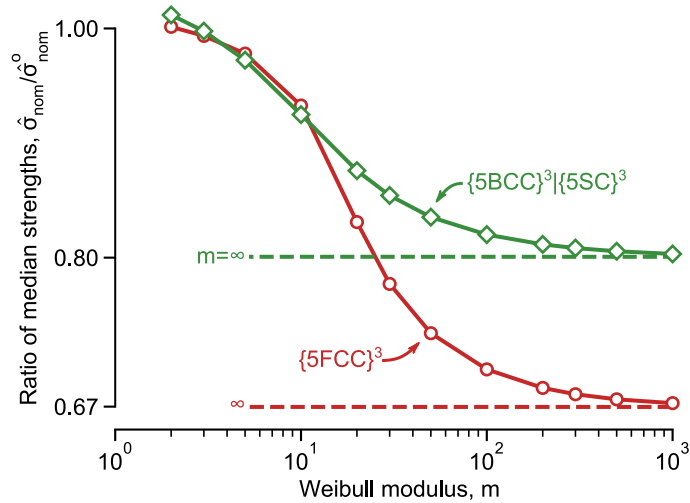


Fig. 11. When strut strength is stochastic, small numbers of highly-strained tensile struts have little effect on median truss strength. For representative values of Weibull moduli of ceramics (say $m = 5 - 10$), the median strength would be reduced by less than 5%.

Distributions of k_i (shown in Fig. 10) range from 0.6 to 1.5 in the $\{FCC\}$ truss and 0.6 to 1.25 in the $\{BCC\}\{SC\}$ truss. The computed ratios of median strengths (in Fig. 11) show that: (i) as $m \rightarrow \infty$, the ratio of median strengths approaches $1/k_{max}$, and (ii) for Weibull moduli typical of structural ceramics ($m = 5 - 10$), the ratios of median strengths are close to unity. (For example, for $m = 5$, the ratios are 0.98 and 0.97 for the $\{FCC\}$ and $\{BCC\}\{SC\}$ trusses, respectively.) The inference is that the small number of affected struts in a large truss made from a brittle material with even a modestly wide strength dispersion should have little effect on average strength.

6. Discussion

Although the present study was based solely on computational modeling, the veracity of the approach has been demonstrated recently through comparisons between numerical predictions and experimental measurements on one specific truss structure. The structure consisted of a $1 \times 2 \times 2$ array of $\{FCC\}$ unit cells, made from a hard thermoplastic by stereolithography (Latture et al., 2018b). In that study, strains had been measured in over 50 individual struts (all that could be imaged externally) in each test specimen by digital image correlation during compressive loading. The computational model had correctly predicted the onset and evolution of strut buckling, identified the transverse struts that experience the highest tensile strain, and predicted the corresponding strut strains.

The present study was also restricted to a single loading scenario: that of uniaxial compressive stress. The use of the modeling approach for other scenarios would require specification of the pertinent boundary conditions as well as truss geometry, characterized by the number and the arrangement of unit cells. To illustrate, we consider design of lightweight sandwich panels comprising a truss core and two thin face sheets. Such panels are attractive for use not only in structural applications but also where additional functionality may be required, e.g. for internal cooling or heat exchange.

Sandwich panels exhibit two fundamental characteristics that differ from those considered here: (i) unit cells are arranged in a planar fashion with, generally, a small number of cells through-thickness and a large number in-plane (in contrast to the cubic arrays analyzed here) and (ii) facesheets strongly constrain deformation of the core. For example, when a uniformly-distributed pressure is applied onto a facesheet of a sandwich panel and the facesheets are sufficiently stiff, the core is subjected to a state of essentially uniaxial compressive *strain* (not stress). Here essentially all of the tensile load that would otherwise be supported by the transverse struts would be supported by the facesheets. But, at the panel edges, these constraints would diminish with distance from the face sheets (measured in multiples of unit cell dimensions). If the core were thick, the peak tensile stresses near the core center would differ substantially from those near the facesheets. Failure prediction in these scenarios would require computational models of the type employed here, incorporating truss size and geometry as well as boundary conditions that reflect constraints of the facesheets. Taking this idea to the limit, cores could be designed in a way that *eliminates* tensile struts altogether. This would be accomplished, for example, with a core comprised of an $\{FCC\}$ truss with only one unit cell in the thickness direction and with the transverse struts on the two faces replaced by facesheets. All struts would therefore be subjected to compression when the panel is loaded externally by pressure.

Although the single-layer core structure may be desirable for mechanical performance, it may not be suitable when other functionality is required. For example, design for effective cooling or heat exchange by passage of a fluid through the core would require consideration of the internal surface area and the dynamics of fluid flow. Here a higher density of smaller

struts would enable more efficient heat transfer, at the expense of larger pressure drops, for a fixed relative density. In turn, a greater number of unit cells would be required to span the distance between the facesheets and therefore the presence of transverse struts would be unavoidable.

7. Conclusions

The key conclusions from this study follow.

1. Among the three trusses studied here, {FCC} is the most defect-tolerant. This is because the strain elevations around bulk strut defects (distant from the free surfaces) are smaller than those at free surfaces. Even when defects are located at a free surface and the strain elevations from the defects are conflated with those due to the surface itself, their effects on local strut strains and compressive truss strength are remarkably small ($\leq 5\%$).
2. Somewhat greater strength reductions are obtained in the binary trusses when defects are situated at the corners (by about 20–25%), a result of the higher strain elevations around these defects.
3. The full strength potential of the {FCC} truss, dictated by large-scale strut buckling, is only attained when the material failure strain exceeds a critical value of $\epsilon_f/\rho \approx 0.25$. This condition is conceivably attainable with hard thermoplastics; a failure strain of $\epsilon_f = 0.05$ would satisfy this condition for relative densities up to $\rho = 0.2$. In contrast, if the truss were made of a high-strength ceramic, where the failure strain (optimistically) may be $\epsilon_f = 0.01$, the condition would only be satisfied for relative densities up to $\rho = 0.04$.
4. When the condition for large-scale buckling is satisfied and the maximum possible strength is attained, the {FCC} truss is preferred over the two binary trusses, since it attains its peak strength at the lowest level of material failure strain. Although in principle the binary {BCC}{SC} truss can achieve a slightly higher strength, this requires materials with much higher failure strains (by almost an order of magnitude). Because of the additional constraints on material properties and the greater geometrical complexity of this truss topology, the marginal strength gains would not likely warrant selection of this truss topology, unless the design necessarily required elastic isotropy in combination with high strength.
5. In cases in which the material failure strain falls well below that required to attain large-scale strut buckling, say $\epsilon_f/\rho < 0.1$, as it might in low relative density ceramic trusses, the {BCC}{SC} truss would be preferred, since it exhibits the highest strength, more than twice that of the {FCC} truss. This is a consequence of the higher truss stiffness and the lower tensile strains generated in the {BCC}{SC} truss.

Acknowledgments

This work was supported by the Institute for Collaborative Biotechnologies through grant W911NF-09-0001 from the U.S. Army Research Office. The content of the information does not necessarily reflect the position or the policy of the Government, and no official endorsement should be inferred.

Supplementary material

Supplementary material associated with this article can be found, in the online version, at doi:10.1016/j.jmps.2018.10.019.

References

- Asadpoure, A., Tootkaboni, M., Valdevit, L., 2017. Topology optimization of multiphase architected materials for energy dissipation. *Comp. Methods Appl. Mech. Eng.* 325, 314–329.
- Bauer, J., Hengsbach, S., Tesari, L., Schwaiger, R., Kraft, O., 2014. High-strength cellular ceramic composites with 3d microarchitecture. *Proceed. Nation. Acad. Sci.* 111 (7), 2453–2458.
- Campoli, G., Borleffs, M., Yavari, S.A., Wauthle, R., Weinans, H., Zadpoor, A.A., 2013. Mechanical properties of open-cell metallic biomaterials manufactured using additive manufacturing. *Materials & Design* 49, 957–965.
- Chen, C., Lu, T., Fleck, N., 1999. Effect of imperfections on the yielding of two-dimensional foams. *J. Mechan. Phys. Solids* 47 (11), 2235–2272.
- Deshpande, V.S., Fleck, N.A., Ashby, M.F., 2001. Effective properties of the octet-truss lattice material. *J. Mechan. Phys. Solids* 49 (8), 1747–1769.
- Evans, A.G., He, M., Deshpande, V.S., Hutchinson, J.W., Jacobsen, A.J., Carter, W.B., 2010. Concepts for enhanced energy absorption using hollow micro-lattices. *Intern. J. Impact Eng.* 37 (9), 947–959.
- Fleck, N.A., Qiu, X., 2007. The damage tolerance of elastic-brittle, two-dimensional isotropic lattices. *J. Mechan. Phys. Solids* 55 (3), 562–588.
- Guo, X.E., Gibson, L.J., 1999. Behavior of intact and damaged honeycombs: a finite element study. *Intern. J. Mech. Sci.* 41 (1), 85–105.
- Gurtner, G., Durand, M., 2014. Stiffest elastic networks. In: *Proc. R. Soc. A*, 470. The Royal Society, p. 20130611.
- Hammett, C.I., Rinaldi, R.G., Zok, F.W., 2013. Pyramidal lattice structures for high strength and energy absorption. *J. Appl. Mech.* 80 (4), 041015.
- Latture, R.M., Begley, M.R., Zok, F.W., 2018a. Design and mechanical properties of elastically isotropic trusses. *J. Mater. Res.* 33 (3), 249–263.
- Latture, R.M., Rodriguez, R.X., Holmes Jr, L.R., Zok, F.W., 2018b. Effects of nodal fillets and external boundaries on compressive response of an octet truss. *Acta Materialia* 149, 78–87.
- Liu, L., Kamm, P., Garcia-Moreno, F., Banhart, J., Pasini, D., 2017. Elastic and failure response of imperfect three-dimensional metallic lattices: the role of geometric defects induced by selective laser melting. *J. Mechan. Phys. Solids* 107, 160–184.
- Liu, X., Liang, N., 2012. Effective elastic moduli of triangular lattice material with defects. *J. Mechan. Phys. Solids* 60 (10), 1722–1739.
- Messner, M.C., 2016. Optimal lattice-structured materials. *J. Mechan. Phys. Solids* 96, 162–183.
- Ostos, J.B., Rinaldi, R., M Hammett, C., Stucky, G., Zok, F., Jacobsen, A., 2012. Deformation stabilization of lattice structures via foam addition. *Acta Materialia* 60 (19), 6476–6485.
- Queheillalt, D., Deshpande, V., Wadley, H., 2007. Truss waviness effects in cellular lattice structures. *J. Mechan. Mater. Struct.* 2 (9), 1657–1675.
- Rinaldi, R., Bernal-Ostos, J., Hammett, C., Jacobsen, A., Zok, F., 2012. Effects of material heterogeneities on the compressive response of thiol-ene pyramidal lattices. *J. Mater. Sci.* 47 (18), 6621–6632.

- Rinaldi, R., Hammetter, C., Zok, F., 2013. Ameliorating property gradients in photocured polymer lattices via thermal curing. *Mater. Lett.* 105, 155–158.
- Salari-Sharif, L., Godfrey, S., Tootkaboni, M., Valdevit, L., 2018. The effect of manufacturing defects on compressive strength of ultralight hollow microlattices: A data-driven study. *Addit. Manufact.* 19, 51–61.
- Silva, M.J., Gibson, L.J., 1997. The effects of non-periodic microstructure and defects on the compressive strength of two-dimensional cellular solids. *Intern. J. Mechan. Sci.* 39 (5), 549–563.
- Symons, D.D., Fleck, N.A., 2008. The imperfection sensitivity of isotropic two-dimensional elastic lattices. *J. Appl. Mechan.* 75 (5), 051011.
- Tancogne-Dejean, T., Spierings, A.B., Mohr, D., 2016. Additively-manufactured metallic micro-lattice materials for high specific energy absorption under static and dynamic loading. *Acta Materialia* 116, 14–28.
- Wadley, H.N., Fleck, N.A., Evans, A.G., 2003. Fabrication and structural performance of periodic cellular metal sandwich structures. *Composit. Sci. Technol.* 63 (16), 2331–2343.
- Wallach, J., Gibson, L.J., 2001. Defect sensitivity of a 3d truss material. *Scripta Materialia* 45 (6), 639–644.
- Zheng, J., Zhao, L., Fan, H., 2012. Energy absorption mechanisms of hierarchical woven lattice composites. *Composit. Part B Eng.* 43 (3), 1516–1522.
- Zok, F.W., 2017. On weakest link theory and weibull statistics. *J. Am. Ceramic Soc.* 100 (4), 1265–1268.
- Zok, F.W., Lattice, R.M., Begley, M.R., 2016. Periodic truss structures. *J. Mechan. Phys. Solids* 96, 184–203.



Ryan M. Lattice is currently a Graduate Student at UCSB. He received his B.S. in Materials Science & Engineering from the University of Tennessee in 2012 and his Ph.D. in Materials from UCSB in 2018. His research focuses on the design of cellular structures with unique mechanical and functional characteristics, including highly-dissipative reversible deformation and tailored elastic/fracture properties.



Matthew R. Begley is currently a Professor of Mechanical Engineering and Professor of Materials at UCSB, having served previously on the faculty at the University of Connecticut (1997–2001) and the University of Virginia (2001–2009). He received his B.S. and M.S. in Mechanical Engineering from Penn State (in 1991 and 1992, respectively) and his Ph.D. in Mechanical Engineering from UCSB in 1995. Begley was a post-doctoral fellow at Harvard University from 1995–1997. Professor Begley's research focus is on theoretical mechanics and advanced simulations to guide materials development, with an emphasis on multilayered systems, interfaces and composites.



Frank W. Zok is currently a Professor of Materials at UCSB. He also serves as Director of the Pratt & Whitney Center of Excellence in Composites at UCSB and has been Associate Editor of the *Journal of the American Ceramic Society* since 1993. He earned B.E.Sc. and M.E.Sc. degrees from the University of Western Ontario and his Ph.D. from McMaster University, Canada, all in Materials Engineering. His research has addressed issues in mechanical and thermal properties of multiphase materials and structures, including ceramic matrix composites, armor ceramics and cermets, mineralized biomaterials, lattices, and various polymer- and metal-matrix composites.